Goal-Oriented High-Order Self-Adaptive *hp*-Finite Element Simulation of Dual-Laterolog Measurements

Myung Jin Nam[1,*], David Pardo[2,*], and Carlos Torres-Verdín[3]

[1]Korea Institute of Geoscience and Mineral Resources (KIGAM), Korea
[2]Basque Center for Applied Mathematics (BCAM), Spain
[3]The University of Texas at Austin, USA
[*]Formerly, at The University of Texas at Austin, USA

Presentation at KSGE, May 6, 2009.

Overview

1. Introduction to a Goal-Oriented High-Order Self-Adaptive hp-Finite Element Method
2. A Fourier Series Expansion in a Non-Orthogonal System of Coordinates
3. Parallel Implementation
4. Introduction to Dual-Laterolog Instruments
5. Numerical Results

Self-Adaptive Goal-Oriented *hp*-FEM

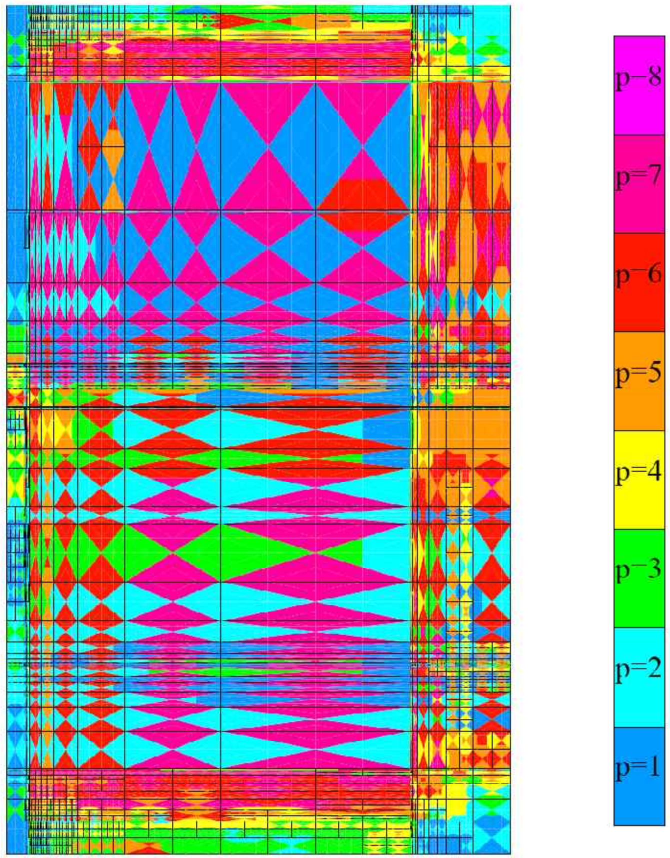

We vary locally the element size *h* and the polynomial order of approximation *p* throughout the grid.

Optimal grids are automatically generated by the *hp*-algorithm.

The self-adaptive goal-oriented *hp*-FEM provides exponential convergence rates in terms of the CPU time vs. the error in a user prescribed quantity of Interest.

DISCRETIZATION

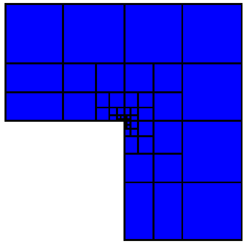

The *h*-Finite Element Method

1. Convergence limited by the polynomial degree, and large material contrasts.
2. Optimal *h*-grids do NOT converge exponentially in real applications.
3. They may "lock" (100% error).

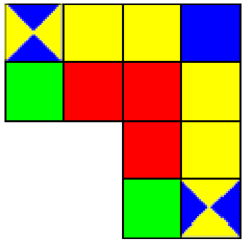

The *p*-Finite Element Method

1. Exponential convergence feasible for analytical ("nice") solutions.
2. Optimal ***p***-grids do NOT converge exponentially in real applications.
3. If initial ***h***-grid is not adequate, the ***p***-method will fail miserably.

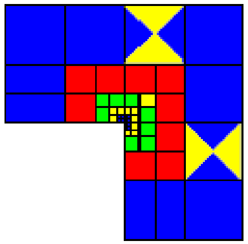

The *hp*-Finite Element Method

1. Exponential convergence feasible for ALL solutions.
2. Optimal ***hp***-grids DO converge exponentially in real applications.
3. If initial ***hp***-grid is not adequate, results will still be great.

DISCRETIZATION I

Energy norm based fully automatic *hp*-adaptive strategy

Coarse grids
(h, p)

Fine grids
($h/2$, $p+1$)

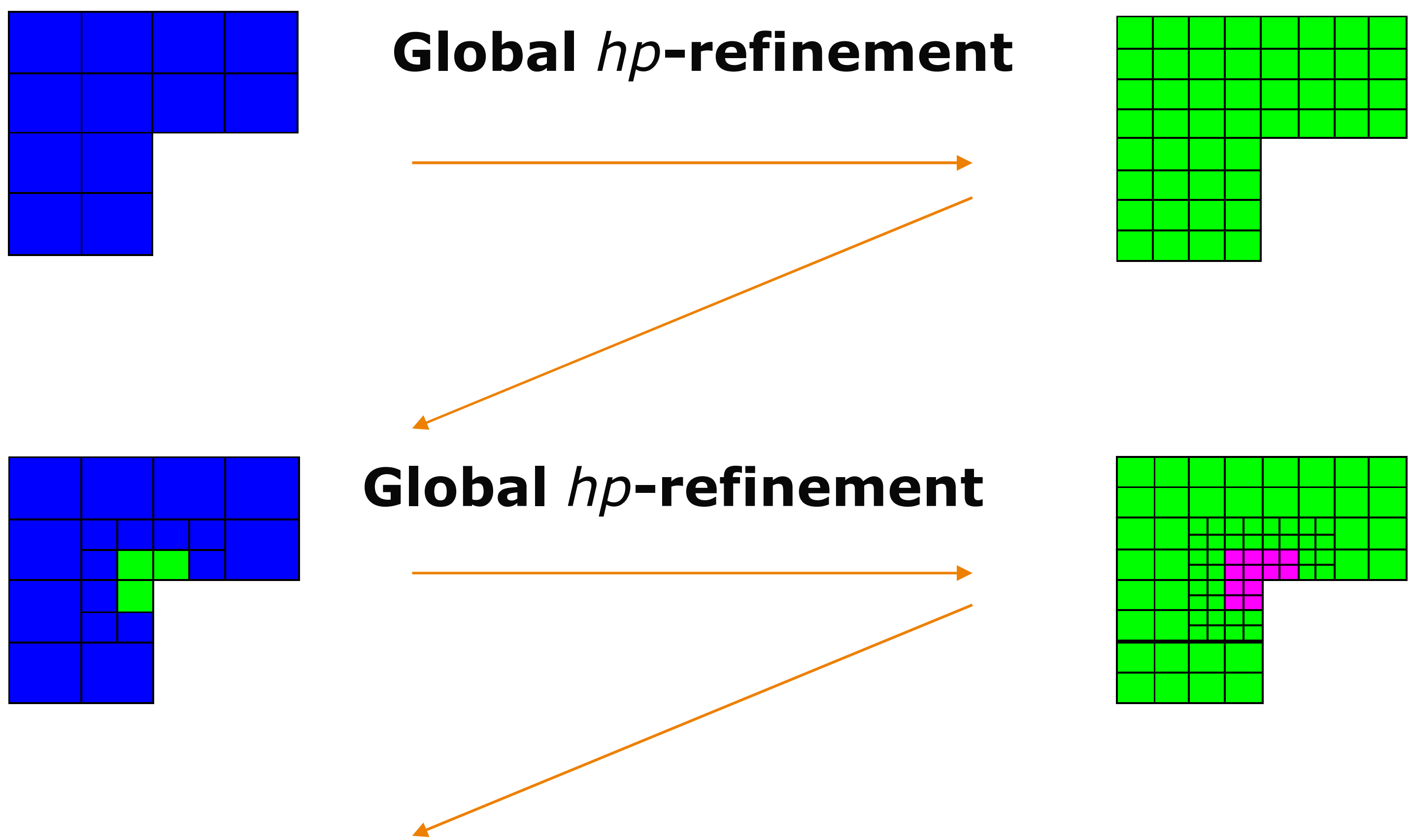

DISCRETIZATION II

Goal-Oriented Adaptivity

Coarse grids
(h, p)

Fine grids
($h/2$, $p+1$)

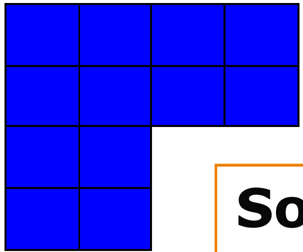

Solve DIRECT (Ψ) and DUAL (G) problems on both grids (h, p) and ($h/2$, $p+1$)

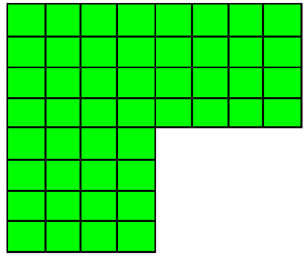

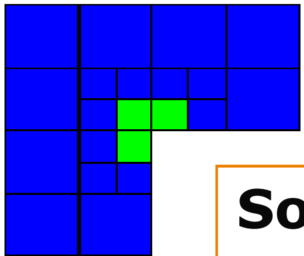

Solve DIRECT (Ψ) and DUAL (G) problems on both grids (h, p) and ($h/2$, $p+1$)

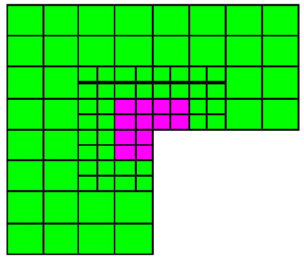

DISCRETIZATION II

Motivation (Goal-Oriented Adaptivity)

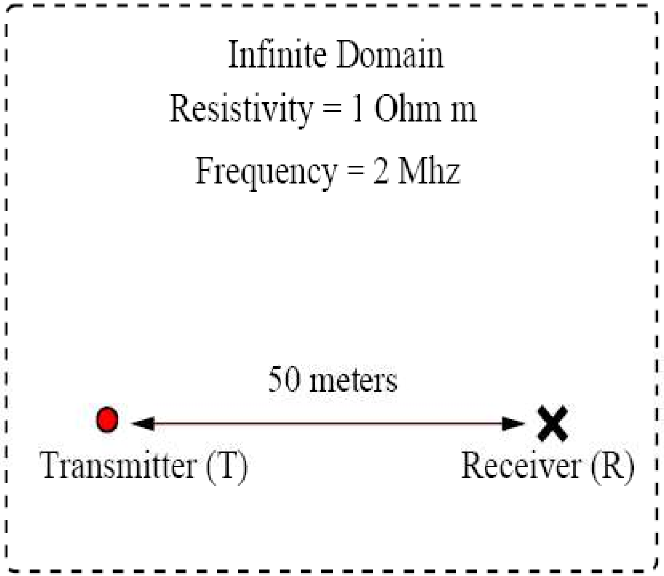

Solution decays exponentially.

$|E(T)|/|E(R)| \approx 10^{60}$

Results using energy-norm adaptivity:

- **Energy-norm error: 0.001%**
- **Relative error in the quantity of interest > 10^{30}%.**

DISCRETIZATION II

Motivation (Goal-Oriented Adaptivity)

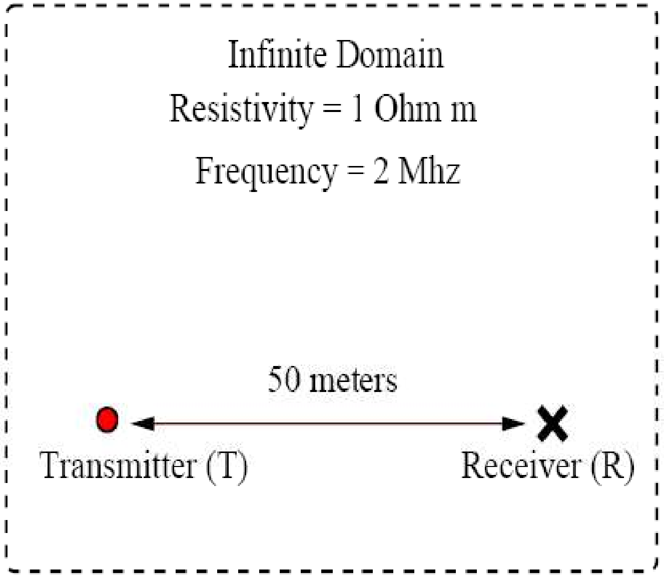

Solution decays exponentially.

$|E(T)|/|E(R)| \approx 10^{60}$

Results using energy-norm adaptivity:

– **Energy-norm error: 0.001%**

– **Relative error in the quantity of interest > 10^{30}%.**

Goal-oriented adaptivity is needed!!!

DISCRETIZATION

Motivation (Goal-Oriented Adaptivity)

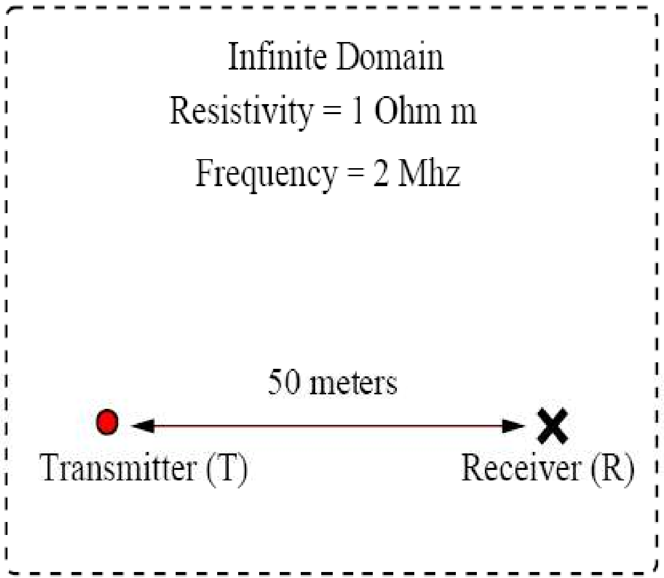

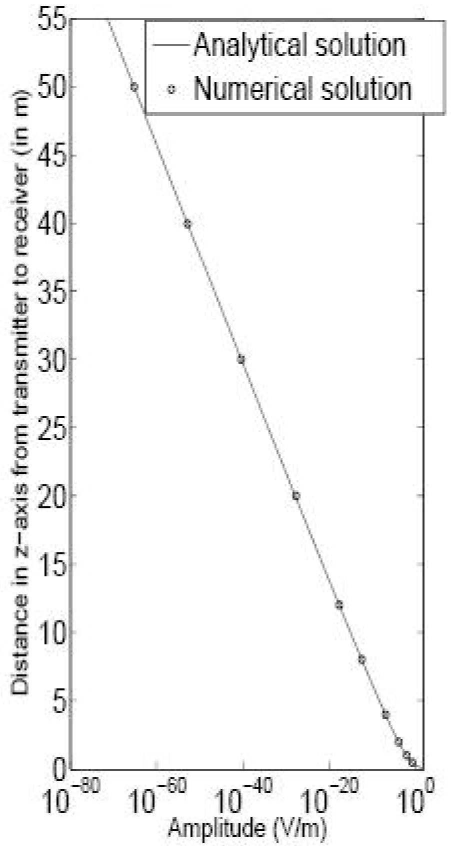

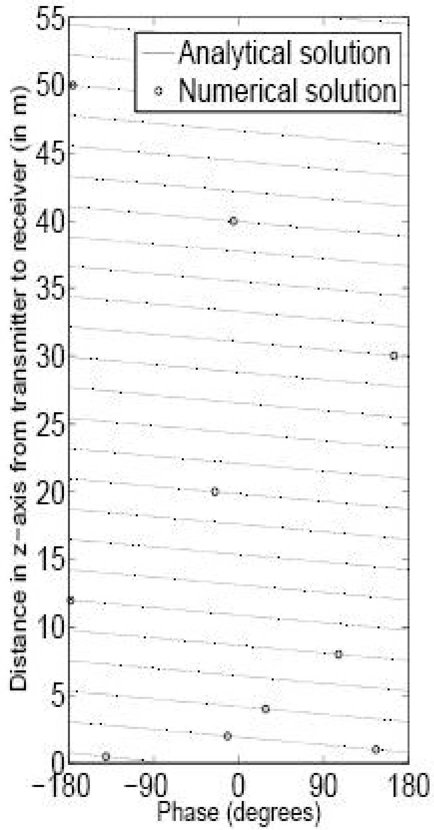

3D Deviated Well

Cartesian system of coordinates: (x_1, x_2, x_3)

New non-orthogonal system of coordinates: $(\zeta_1, \zeta_2, \zeta_3)$

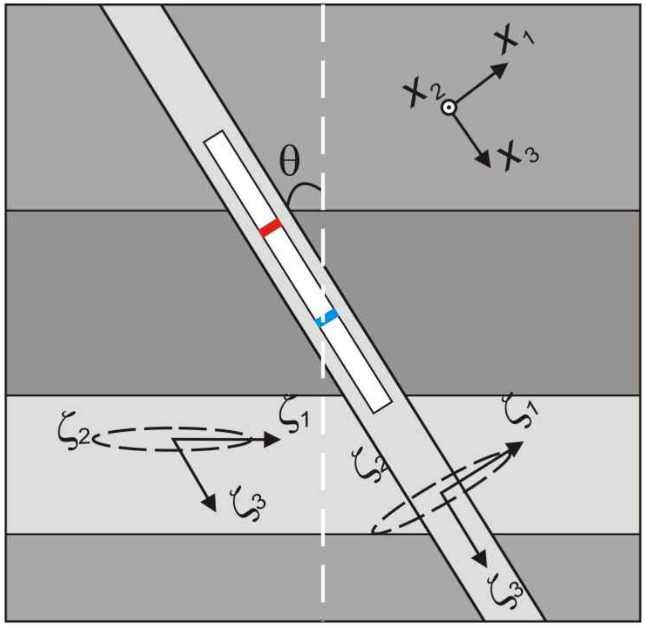

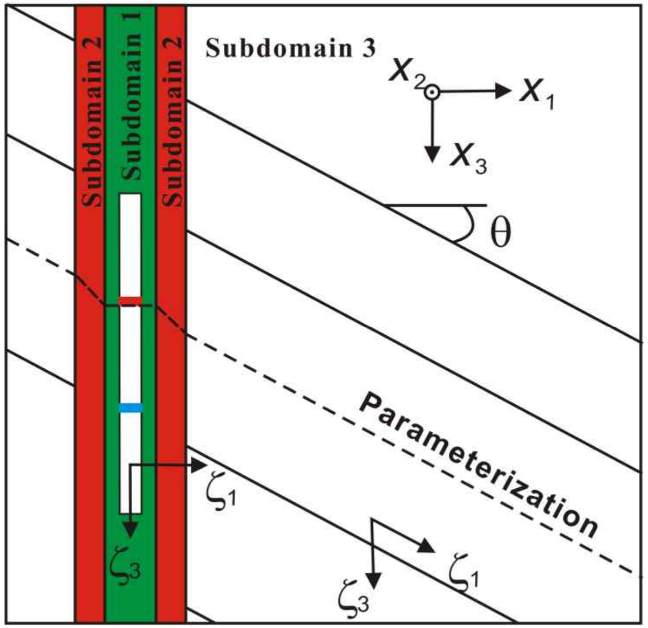

Subdomain 1

$$\begin{cases} x_1 = \zeta_1 \cos \zeta_2 \\ x_2 = \zeta_1 \sin \zeta_2 \\ x_3 = \zeta_3 \end{cases}$$

Subdomain 2

$$\begin{cases} x_1 = \zeta_1 \cos \zeta_2 \\ x_2 = \zeta_1 \sin \zeta_2 \\ x_3 = \zeta_3 + \tan\theta \dfrac{\zeta_1 - \rho_1}{\rho_2 - \rho_1} \rho_2 \cos \zeta_2 \end{cases}$$

Subdomain 3

$$\begin{cases} x_1 = \zeta_1 \cos \zeta_2 \\ x_2 = \zeta_1 \sin \zeta_2 \\ x_3 = \zeta_3 + \zeta_1 \tan\theta \cos \zeta_2 \end{cases}$$

3D Deviated Well

Cartesian system of coordinates: (x_1, x_2, x_3)

New non-orthogonal system of coordinates: $(\zeta_1, \zeta_2, \zeta_3)$

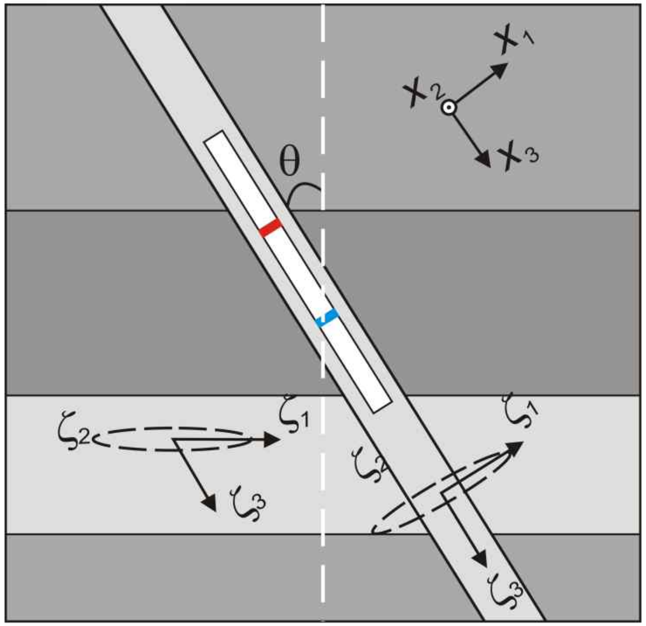

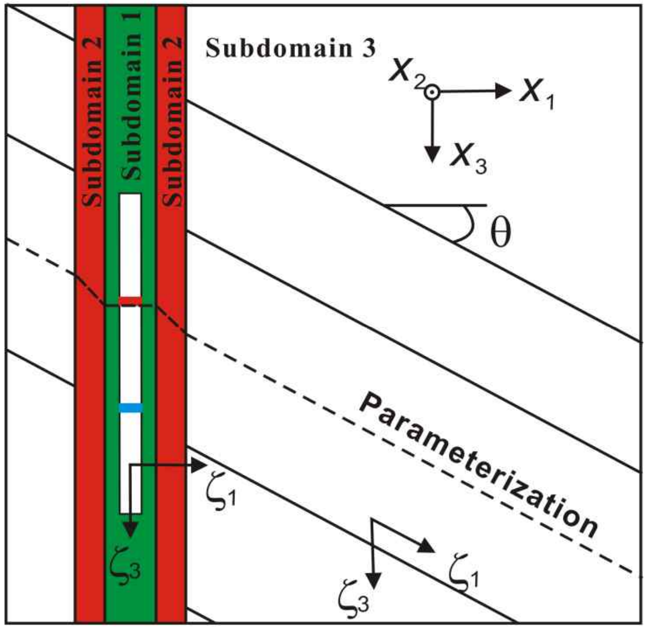

Constant material coefficients in the quasi-azimuthal direction ζ_2 in the new non-orthogonal system of coordinates!!!!

3D Deviated Well

For each Fourier mode, we obtain a 2D problem. Each 2D problem couples with up to five different 2D problems corresponding to different Fourier modes, therefore, constituting the resulting 3D problem.

When we use 9 Fourier modes for the Solution:

$$\begin{bmatrix} A_{1,1} & A_{1,2} & A_{1,3} & 0 & 0 & 0 & 0 & 0 & 0 \\ A_{2,1} & A_{2,2} & A_{2,3} & A_{2,4} & 0 & 0 & 0 & 0 & 0 \\ A_{3,1} & A_{3,2} & A_{3,3} & A_{3,4} & A_{3,5} & 0 & 0 & 0 & 0 \\ 0 & A_{4,2} & A_{4,3} & A_{4,4} & A_{4,5} & A_{4,6} & 0 & 0 & 0 \\ 0 & 0 & A_{5,3} & A_{5,4} & A_{5,5} & A_{5,6} & A_{5,7} & 0 & 0 \\ 0 & 0 & 0 & A_{6,4} & A_{6,5} & A_{6,6} & A_{6,7} & A_{6,8} & 0 \\ 0 & 0 & 0 & 0 & A_{7,5} & A_{7,6} & A_{7,7} & A_{7,8} & A_{7,9} \\ 0 & 0 & 0 & 0 & 0 & A_{8,6} & A_{8,7} & A_{8,8} & A_{8,9} \\ 0 & 0 & 0 & 0 & 0 & 0 & A_{9,7} & A_{9,8} & A_{9,9} \end{bmatrix} \begin{bmatrix} x_1 \\ x_2 \\ x_3 \\ x_4 \\ x_5 \\ x_6 \\ x_7 \\ x_8 \\ x_9 \end{bmatrix} = \begin{bmatrix} b_1 \\ b_2 \\ b_3 \\ b_4 \\ b_5 \\ b_6 \\ b_7 \\ b_8 \\ b_9 \end{bmatrix}$$

$A_{i,j}$: represents a full 2D problem for each Fourier basis function

Parallelization Implementation

Distributed Domain Decomposition

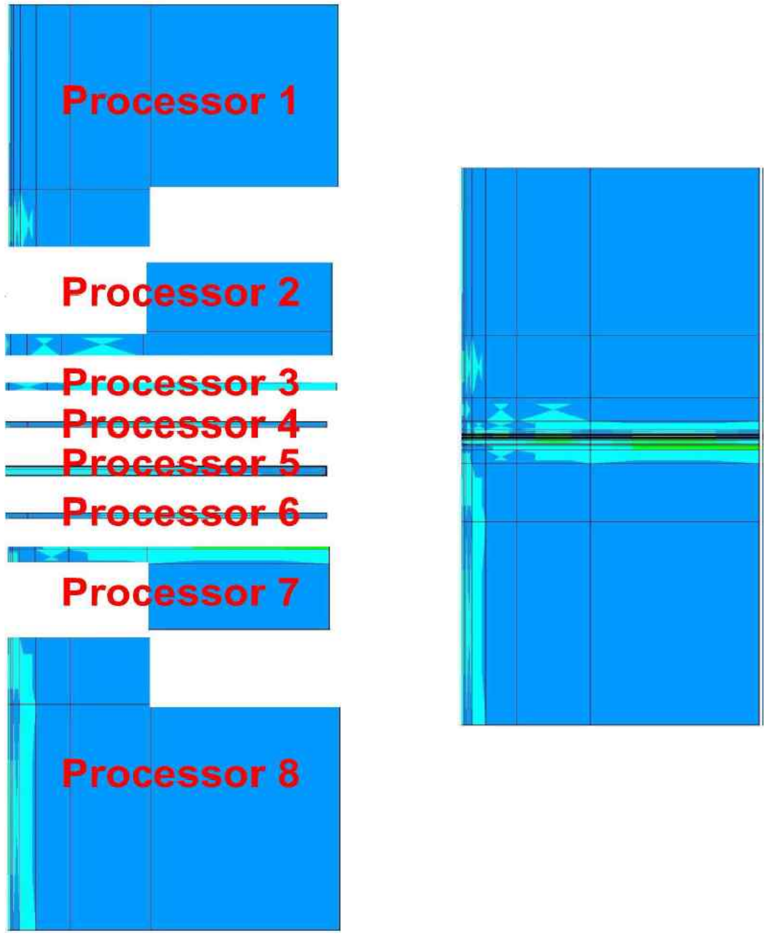

Shared Domain Decomposition!!

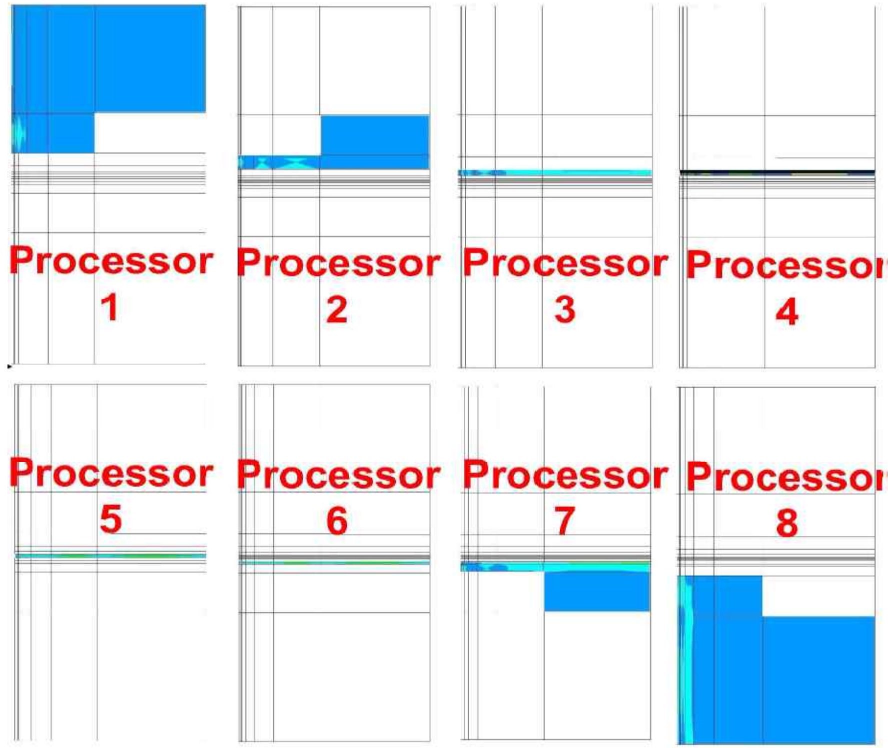

Dual Laterolog (DLL)

- **Determination of Intensities (W_i) of Bucking Currents**

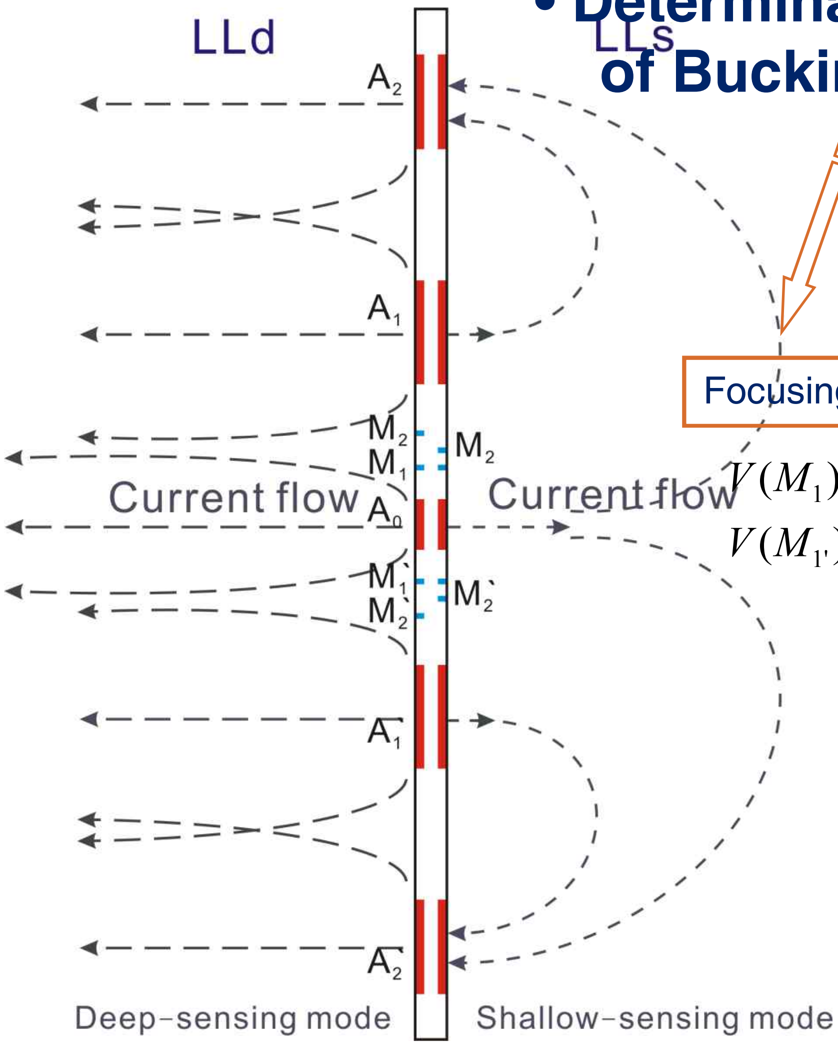

Focusing Conditions

$$V(M_1) = V(M_2)$$

$$V(M_{1'}) = V(M_{2'})$$

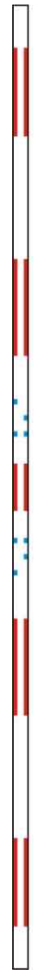

Post-Processing Method

Synthetic Focusing (Cozzolino et al, 2007)

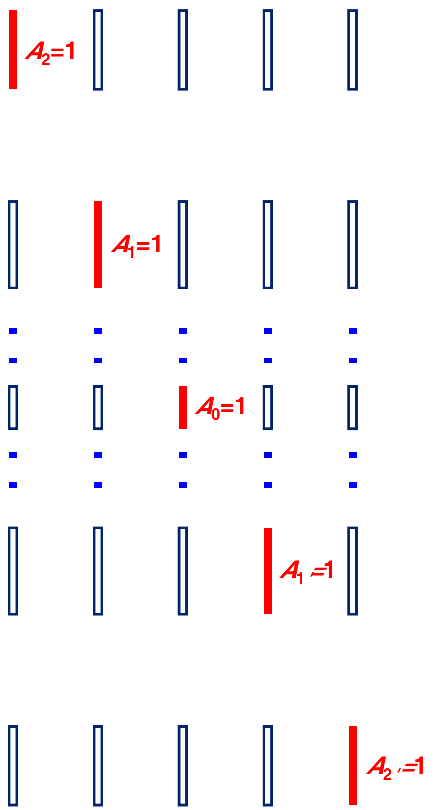

(1) Focusing conditions

$$V(M_1) = V(M_2)$$
$$V(M_{1'}) = V(M_{2'})$$

(2) Relationships between W_j

$$W_2 = (W_1 + c), \quad W_{2'} = (W_{1'} + c) \quad for \ \text{LLd}$$
$$W_2 = -(W_1 + c), \quad W_{2'} = -(W_{1'} + c) \quad for \ \text{LLs}$$

with $c = 0.5$

Total potential on M_j

→ Superposition principle

$$V(M_2) = W_2 V_{2,2} + W_1 V_{2,1} + V_{2,0} + W_{1'} V_{2,1'} + W_{2'} V_{2,2'}$$
$$V(M_1) = W_2 V_{1,2} + W_1 V_{1,1} + V_{1,0} + W_{1'} V_{1,1'} + W_{2'} V_{1,2'}$$
$$V(M_{1'}) = W_2 V_{1',2} + W_1 V_{1',1} + V_{1',0} + W_{1'} V_{1',1'} + W_{2'} V_{1',2'}$$
$$V(M_{2'}) = W_2 V_{2',2} + W_1 V_{2',1} + V_{2',0} + W_{1'} V_{2',1'} + W_{2'} V_{2',2'}$$

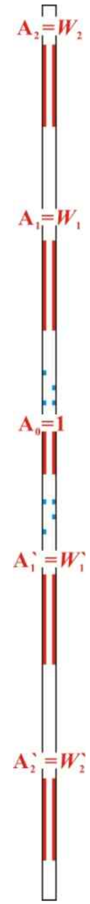

W_j for LLd: < from (1) and (2) with the LLd relationship of (3) >

$$\begin{bmatrix} V_{1,2}+V_{1,1}-V_{2,2}-V_{2,1} & V_{1,1'}+V_{1,2'}-V_{2,1'}-V_{2,2'} \\ V_{2',2}+V_{2',1}-V_{1',2}-V_{1',1} & V_{2',1'}+V_{2',2'}-V_{1',1'}-V_{1',2'} \end{bmatrix} \begin{bmatrix} W_1 \\ W_{1'} \end{bmatrix} = \begin{bmatrix} V_{2,0}-V_{1,0}+c(V_{2,2}+V_{2,2'}-V_{1,2}-V_{1,2'}) \\ V_{1',0}-V_{2',0}+c(V_{1',2}+V_{1',2'}-V_{2',2}-V_{2',2'}) \end{bmatrix}$$

W_j for LLs: < from (1) and (2) with the LLs relationship of (3) >

$$\begin{bmatrix} V_{2,2}+V_{1,1}-V_{2,1}-V_{1,2} & V_{2,2'}+V_{1,1'}-V_{1,2'}-V_{2,1'} \\ V_{1',2}+V_{2',1}-V_{1',1}-V_{2',2} & V_{1',2'}+V_{2',1'}-V_{2',2'}-V_{1',1'} \end{bmatrix} \begin{bmatrix} W_1 \\ W_{1'} \end{bmatrix} = \begin{bmatrix} V_{2,0}-V_{1,0}+c(V_{2,2}+V_{2,2'}-V_{1,2}-V_{1,2'}) \\ V_{1',0}-V_{2',0}+c(V_{1',2}+V_{1',2'}-V_{2',2}-V_{2',2'}) \end{bmatrix}$$

One problem with several RHSs

Embedded Post-Processing Method (EPPM)

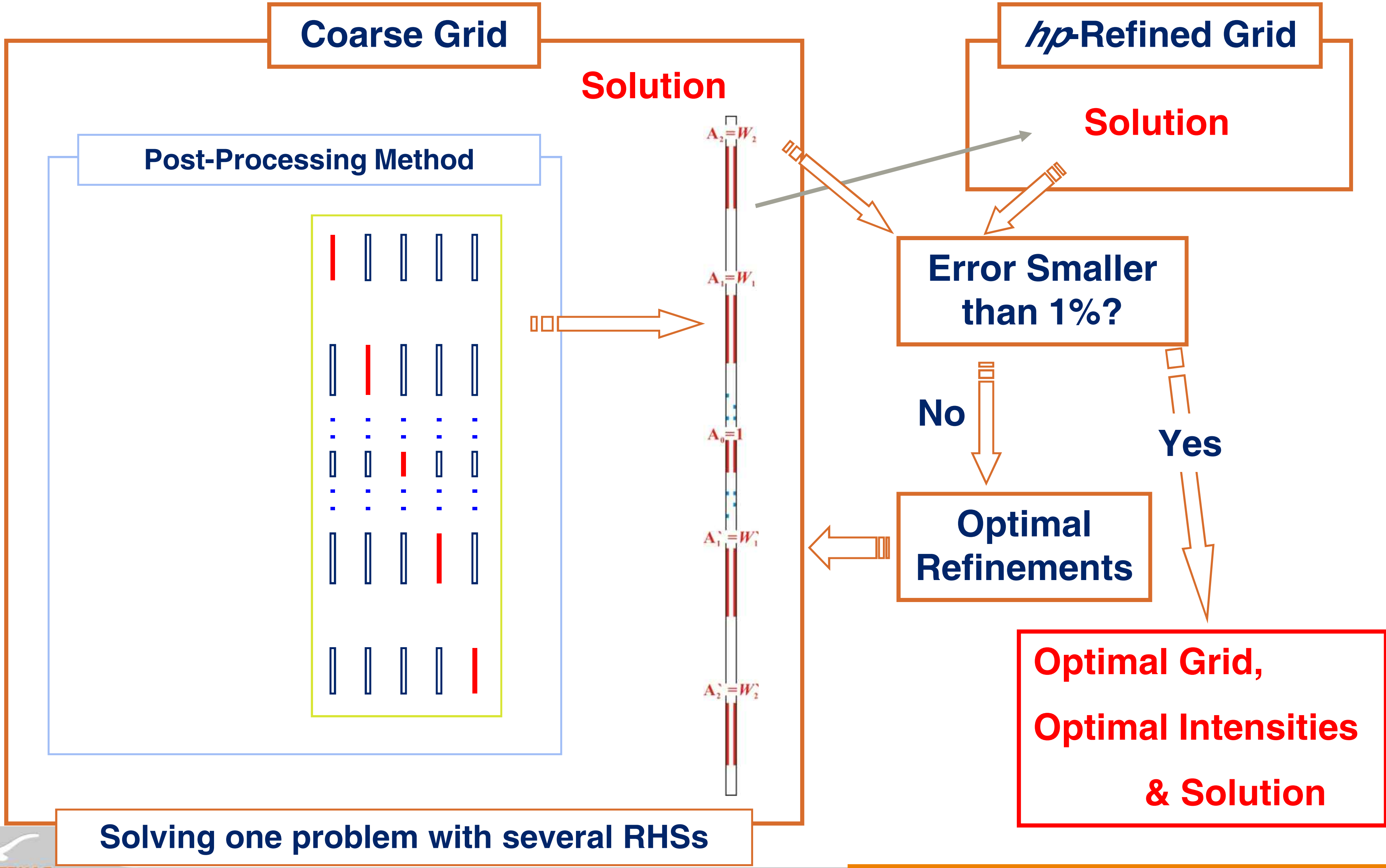

Modeled DLL tool

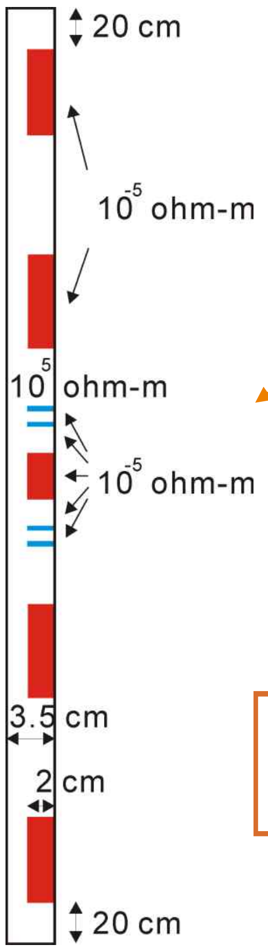

The resistivities and radial lengths of electrode and mandrel.

The vertical dimensions and locations of each electrode:
We followed the vertical tool configuration of a commercial tool

Invaded Formation

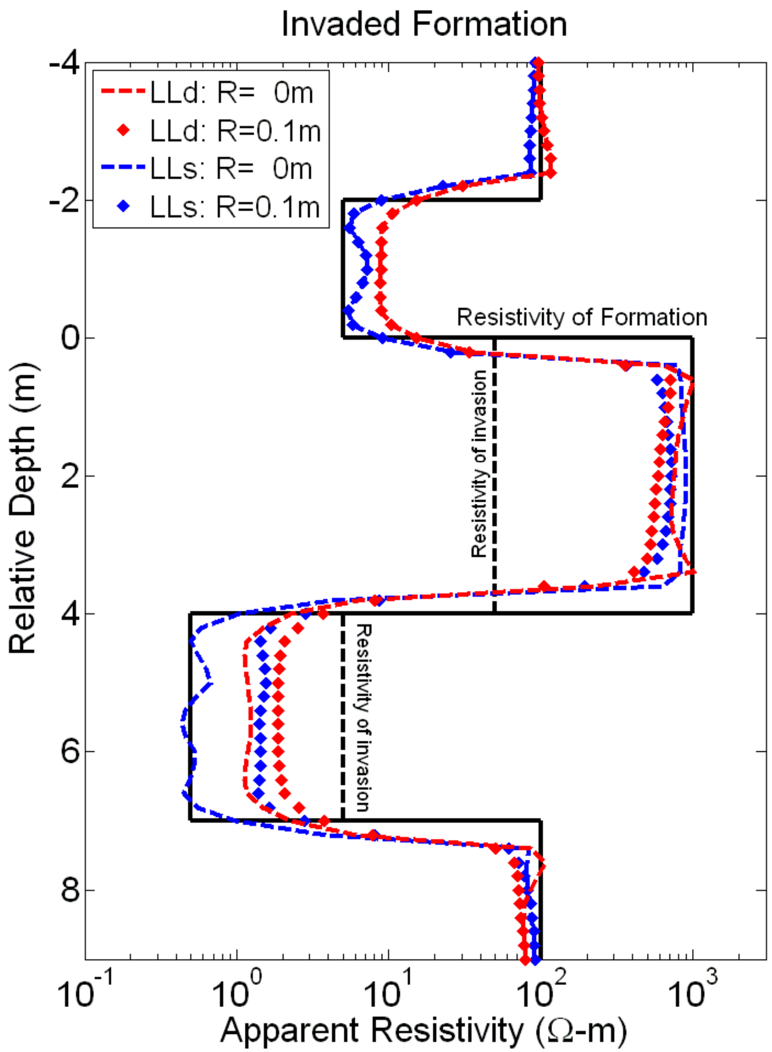

Effects of Invasion: LLs ↑

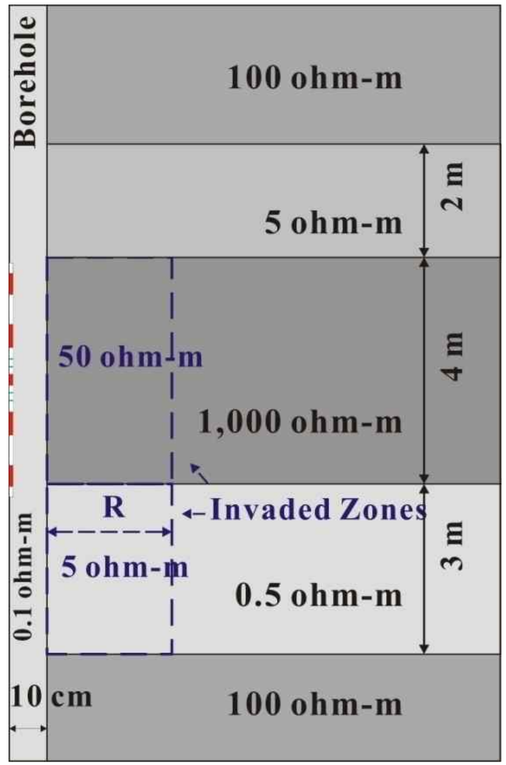

Borehole: 0.1 m in radius

0.1 ohm-m in resistivity

Anisotropic Formation

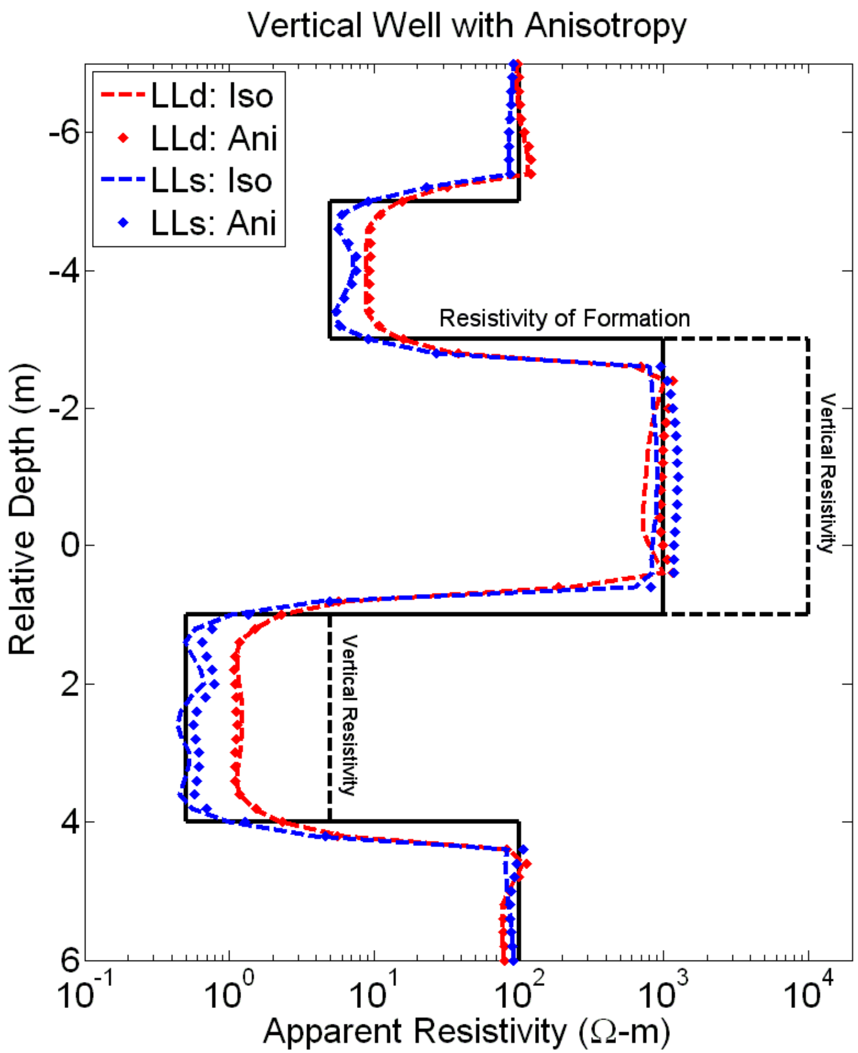

Effects of anisotropy: LLs ↑

LLd: effects of anisotropy are negligible in conductive layer

Deviated Wells

0, 10, 45, and 60 degrees

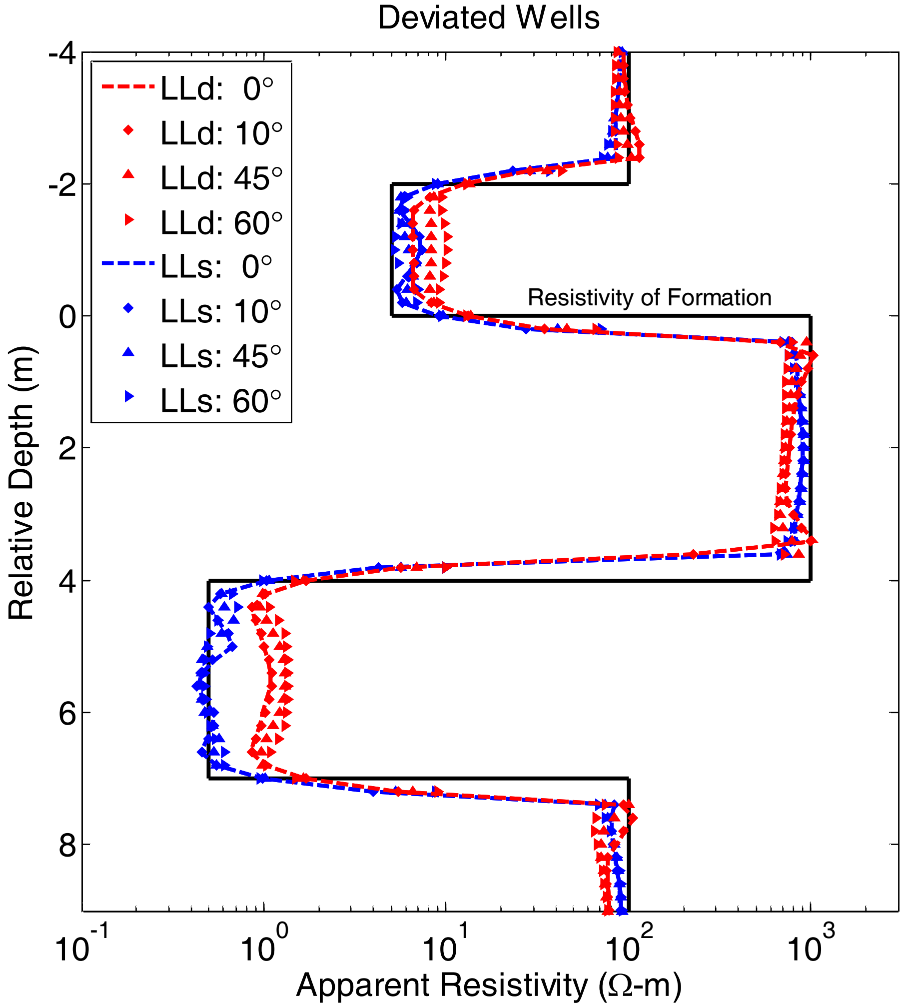

Effects of dip angle:
Thin layer ↑

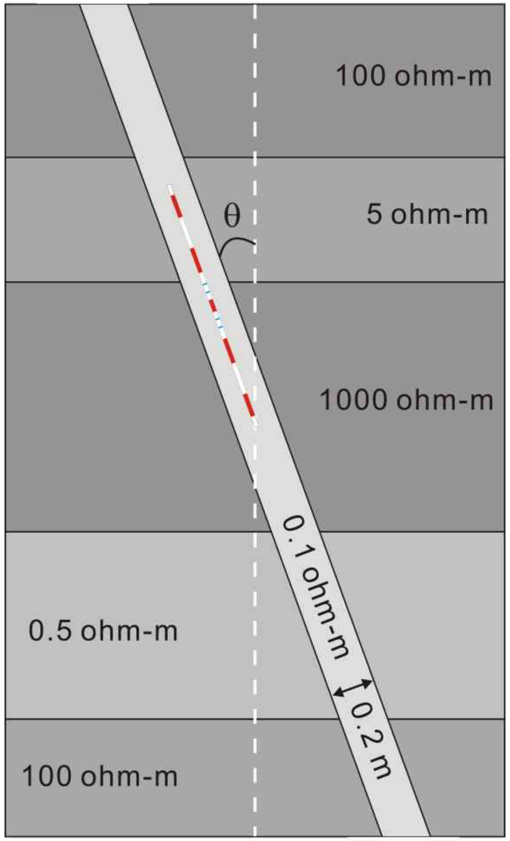

Anisotropic Formation

60- and 0-degree Deviated Wells

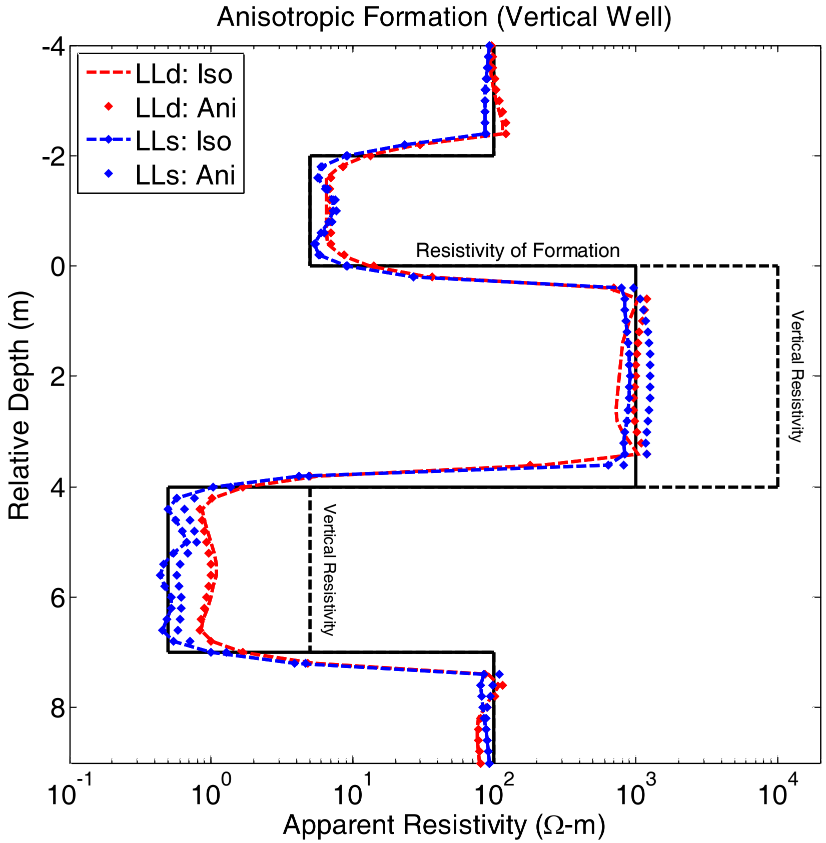

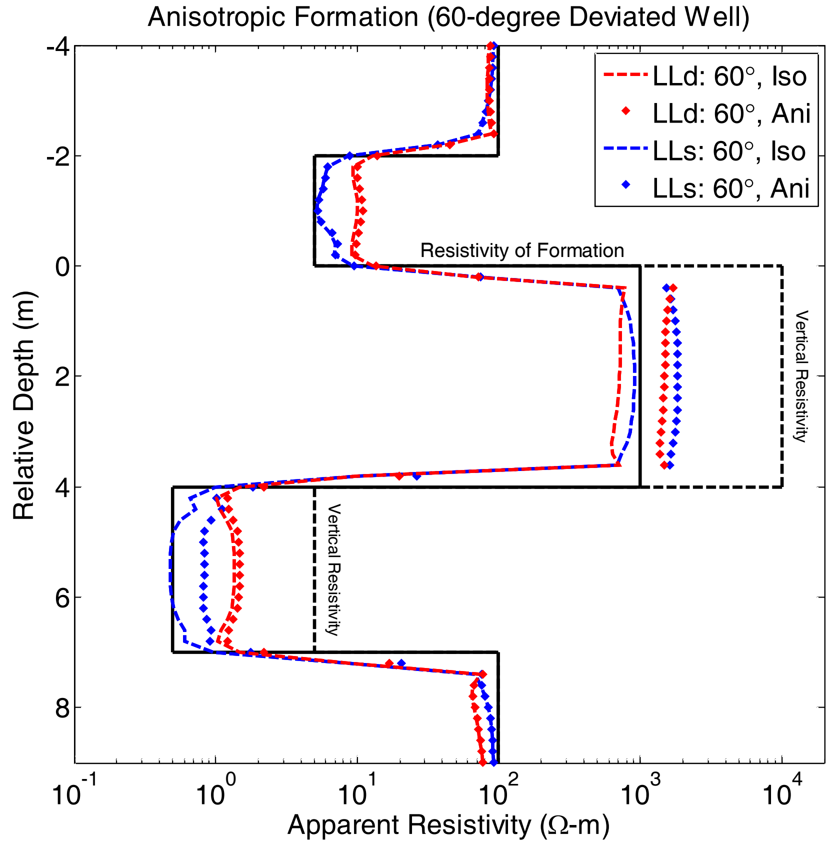

Effects of anisotropy increase with increase of dip angle

Conclusions

- We have successfully simulated 3D dual-laterolog measurements by combining the use of a Fourier series expansion in a non-orthogonal system of coordinates with a 2D higher-order self-adaptive hp finite element method.
- We have generated optimal hp finite element grids and optimal intensities of currents for simulation of dual-laterolog measurements using an embedded post-processing technique in the hp finite element method.
- Effects of dip angle are larger in conductive layers than in resistive layers.
- Effects of anisotropy increase as dip angle increases.

Acknowledgements

The work reported in this paper was funded by UT Austin's consortium on Formation Evaluation sponsored by :

Acknowledgements

The work reported in this paper was also funded by the Ministry of Land, Transport and Maritime Affairs of Korea.

The work of the second author was partially funded by the Spanish Ministry of Science and Innovation under the projects MTM2008-03541 and TEC2007-65214.